Optics Communications 296 (2013) 17–24

Contents lists available at SciVerse ScienceDirect

Optics Communications

journal homepage: www.elsevier.com/locate/optcom

The simultaneous suppression of phase shift error and harmonics in the phase shifting interferometry using carrier squeezing interferometry

Bo Li [a,b,*], Lei Chen [c], Chen Xu [a,b], Jinpeng Li [c]

[a] Nanjing Institute of Astronomical Optics & Technology, Chinese Academy of Sciences, Nanjing 210042, China
[b] Key Laboratory of Astronomical Optics & Technology, Nanjing Institute of Astronomical Optics & Technology, Chinese Academy of Sciences, Nanjing 210042, China
[c] School of Electronic Engineering & Optoelectronic Technology, Nanjing University of Science & Technology, Nanjing 210094, China

ARTICLE INFO

Article history:
Received 12 October 2012
Received in revised form
4 January 2013
Accepted 20 January 2013
Available online 13 February 2013

Keywords:
Optical testing
Phase shifting interferometry
Phase shift error
Harmonics

ABSTRACT

The phase shift errors and the harmonics are the most common types of errors in the phase shifting interferometry. Although there are many suppression techniques for these two errors, it is hard to suppress them simultaneously. In this paper the carrier squeezing interferometry is used to solve this problem, where the data of phase shifting interferograms with linear carrier are re-arranged to acquire a spatial–temporal fringes image. In the frequency domain of the image the lobes of harmonics and phase shift errors and the lobe of the phase are separated, so the correct phase can be extracted by filtering. The algorithm is validated by both simulations and the experiments, with the phase retrieving accuracy greater than $\lambda/400$ and $\lambda/200$ (RMS value), respectively. The spatial uniform phase shift errors and harmonics can be suppressed by this method, using only four phase shifting interferograms.

1. Introduction

The phase shifting interferometry (PSI) is widely used in optical testing for its precision, automation and the ability to obtain the global phase [1]. In the PSI two conditions should be satisfied to ensure the precision of phase retrieving: (1) the phase shift values between the interferograms are accurate, and (2) the interferogram intensity is an ideal sine modulation of the phase. However, in the actual measurements, the phase shift error is caused by vibrations and phase shifter distortion, while the non-sinusoid interferogram intensity is caused by the detector non-linear, the multi-reflective interferences or the image saturation [2].

To solve these problems, many error suppression algorithms are proposed, which can be divided into three classes: (1) In the error insensitive phase shift algorithms [3–5], the sample weights of the signal in the phase retrieving calculation are designed to make them insensitive to some harmonics and the phase shift error with special form, but usually the orders of phase shift distortion cannot be greater than two. (2) In the phase shift calibration algorithms, the inaccurate phase shift values are considered as the unknowns and solved by iterative [6–8] or non-iterative [9,10] methods, and then the phase is reconstructed by the least square calculation. Various kinds of phase shift errors can be suppressed in this class of methods, however, the effect of harmonics cannot be eliminated. (3) In the error compensation algorithms [11–13], the inaccurate retrieved phase are compensated to get the right one, guided by the specific phase errors caused by the related error sources (vibrations, for example). Unfortunately, the harmonics rejection is still unavailable in these methods. On the other hand, some methods to calibrate or reject the harmonics of the fringes are proposed [14–16], but they cannot suppress the phase shift errors at the same time. Considering the coupling of these two kinds of errors, they should be suppressed simultaneously while not calibrated one by one. Therefore, Xu [17] and Hoang [18] proposed two advanced iterative algorithms, by which the two errors can be suppressed simultaneously. But in their methods $2p+1$ frames of phase shifting interferograms are necessary if the pth order harmonic is needed to reject.

In this paper, the carrier squeezing interferometry (CSI) algorithm is used to suppress the phase shift error and harmonics simultaneously to retrieve the accurate phase. CSI is a phase retrieving algorithm we proposed [19] to retrieve the phase in PSI, which is a modified algorithm arising from the squeezing interferometry (SI) algorithm proposed by Servin et al. [20]. Compared to the SI, all spatial uniform phase shift errors within the magnitude of $\pm 15^\circ$ and harmonics can be suppressed well (with the cost of blurring some information with high frequency), but its error suppression ability is only demonstrated under the condition of the simple sinusoid model (without harmonics) in

* Corresponding author at: Chinese Academy of Sciences, Nanjing Institute of Astronomical Optics & Technology, Bancang Street, 188#, Nanjing 210042, China. Tel.: +86 2 585430617.
E-mail addresses: bli@niaot.ac.cn, 542134007@qq.com (B. Li).

0030-4018/$ - see front matter © 2013 Elsevier B.V. All rights reserved.
http://dx.doi.org/10.1016/j.optcom.2013.01.060

our early work. On the other hand, although the harmonics rejection feature of SI and the analogous methods has been researched by Servin and Padilla et al. [20,21], the phase shift errors are not discussed except for the detuning error. That is, the situation with both phase shift errors and harmonics in the SI–CSI frame has not been studied. Therefore, in this paper the more general phase shifting interferograms model with random phase shift error and non-sinusoid signal is used to analyze the property of CSI, and its ability to suppress the phase shift errors and harmonics simultaneously will be validated by theory, simulations and experiments. Different from the algorithms of Xu and Hoang, only four frames of phase shifting interferograms are necessary in the CSI and the iterative calculation can be evaded.

1. Principle

Usually a phase shifting interferogram can be written as

$$s_m(x,y) = b_0 + b_1\cos[\varphi(x,y) + 2\pi m f_0 + r_m] \tag{1}$$

where x and y are the spatial coordinates, the subscript m represents the mth interferogram, b_0 is the background intensity, b_1 is the contrast, φ is the unknown phase, r_m represents the phase shift error, f_0 is the temporal phase shift frequency ($f_0=1/4$ for most commercial phase shifting interferometers in the normalized frequency domain coordinate). However, the fringes will not be sinusoidal as presented by Eq. (1) caused by some factors in the actual measurements such as the nonlinear response of the detector, the intensity saturation and multi-reflective interferences. In these situations, the interferogram is periodic but not sinusoidal, that is, the high order harmonics exist; and an interferogram with high order harmonics can be represented by

$$s_m(x,y) = \sum_{k=0}^{\infty} b_k\{\cos k[\varphi(x,y) + 2\pi m f_0 + r_m]\} \tag{2}$$

where b_k is the coefficient of the kth harmonics. In the CSI method, the data of phase shifting interferograms are re-arranged by row or column to be fused into a frame of spatial–temporal fringes (STF) which contains not only the spatial phase information but also the temporal phase shift information. In this paper the data is re-arranged by column, that is:

$$s'(Mx+m,y) = s_m(x,y) \tag{3}$$

where M is the amount of the interferograms and

$$f_0 = \frac{1}{M} \tag{4}$$

And the intensity of STF is:

$$s'(x',y) = \sum_{k=0}^{\infty} b_k\{\cos k[\varphi'(x',y) + 2\pi f_0 x' + p(x',y)]\} \tag{5}$$

where x' is the spatial coordinate after extension and the error term $p(x', y)$ is given by

$$p(x',y) = \sum_{m=0}^{M-1}\sum_{n=-N/2}^{N/2-1} r_m\delta(x'-Mn-m,y) \tag{6}$$

where n represents the nth column in the original interferograms (with the width of N columns). Moreover, $\varphi(x', y)$ is the extended phase of $\varphi(x,y)$ along the x direction, which is

$$\varphi'\left(\left[\frac{x'}{M}\right]_{\text{int}}, y\right) = \varphi(x,y) \tag{7}$$

and $[\cdot]$int is the operator to get the integer. In Fig. 1(a) and (b) one of the phase shifting interferograms and the re-arranged STF image are given as an example, but the left half of the STF image is shown in Fig. 1(b) since the width of the whole image is too large.

Since the phase shift error r_m is usually a small value compared with the phase shift period, the first-order approximation can be used to get

$$s'(x',y) = s_0 + \sum_{k=1}^{\infty} s_{+k} + \sum_{k=1}^{\infty} s_{-k} + \sum_{k=1}^{\infty} e_{+k} + \sum_{k=1}^{\infty} e_{-k} \tag{8}$$

where the background is

$$s_0 = b_0 \tag{9}$$

and the $\pm k$th order of signal is

$$s_{\pm k}(x',y) = \frac{b_k}{2}\exp[\pm ik(2\pi f_0 x' + \varphi')] \tag{10}$$

while the $\pm k$th order of error is

$$e_{\pm k}(x',y) = \mp s_{\pm k}(x',y) \times k\sum_{m=0}^{M-1}\sum_{n=-\infty}^{\infty} r_m\delta(x'-Mn-m,y) \tag{11}$$

Then we can obtain the frequency spectrum by using spatial 2-D Fourier transform (FT) to Eq. (8), which is written as

$$S(f_x,f_y) = S_0 + \sum_{k=1}^{\infty} S_{+k} + \sum_{k=1}^{\infty} S_{-k} + \sum_{k=1}^{\infty} E_{+k} + \sum_{k=1}^{\infty} E_{-k} \tag{12}$$

where the background lobe is the FT of Eq. (9):

$$S_0 = b_0 \times \delta(0,0) \tag{13}$$

and the $\pm k$th-order lobe of phase is the FT of Eq. (10):

$$S_{\pm k} = \frac{b_k}{2}\Phi_{\pm k}(f_x \mp kf_0, f_y) \tag{14}$$

while the $\pm k$th-order lobe of error is the FT of Eq. (11):

$$E_{\pm k} = \frac{\mp k}{M}\sum_{m=0}^{M-1} r_m \sum_{n=-\infty}^{\infty}\exp(-i2\pi mnf_0)S_{\pm k}(f_x - nf_0, f_y) \tag{15}$$

And in Eq. (14) $\Phi_{\pm k}(f_x, f_y)$ is defined by

$$\Phi_{\pm k}(f_x,f_y) = FT[\exp(\pm ik\varphi')] \tag{16}$$

where the operator $FT[\cdot]$ represents the Fourier transform.

From Eq. (12) it can be seen that the spectrum of STF is composed by the background lobe $S0$, the $\pm k$th phase lobes $S_{\pm k}$ and the $\pm k$th error lobes $E_{\pm k}$. To reconstruct the phase correctly, the $S+1$ (or $S-1$) lobe should be extracted independently, so the lobes with the potential of overlapping with $S+1$ will be analyzed as follows. First, there is no overlapping between any two adjacent lobes of $S_{\pm k}$ because the distance between them is always f_0 which is a large value (1/4 of the total length of the frequency domain coordinate for the phase shift interval $\pi/2$). Second, from Eq. (15) we can know that the error spectrum $E_{\pm k}$ composed by a series of lobes with the interval of f_0 and the central location of $\pm kf_0$, therefore, the error lobes which may overlap with $S+1$ are

$$E_{+k}\big|_{n=k-1} = \frac{-k}{M}\sum_{m=0}^{M-1} r_m\exp[-i2\pi m(k-1)f_0]S_{+k}[f_x-(k-1)f_0,f_y] \tag{17}$$

and

$$E_{-k}\big|_{n=k+1} = \frac{+k}{M}\sum_{m=0}^{M-1} r_m\exp[-i2\pi m(k+1)f_0]S_{-k}[f_x-(k+1)f_0,f_y] \tag{18}$$

To evade the overlapping of the phase lobe and error lobe in CSI method, a linear carrier is introduced in the original phase shifting interferograms [19], and in the following analysis we will demonstrate that this condition is still effective when there are high order harmonics. Assuming that the carrier f_c is introduced

along y direction, then Eq. (14) is changed to

$$S_{\pm k} = \frac{b_k}{2}\Phi_{\pm k}(f_x \mp kf_0, f_y \mp kf_c) \tag{19}$$

Correspondingly, Eqs. (17) and (18) are re-written as

$$E_{+k,n=k-1} = \frac{-k}{M}\sum_{m=0}^{M-1} r_m \exp[-i2\pi m(k-1)f_0]S_{+k}(f_x, f_y) \tag{20}$$

and:

$$E_{-k,n=k+1} = \frac{+k}{M}\sum_{m=0}^{M-1} r_m \exp[-i2\pi m(k+1)f_0]S_{-k}[f_x-(k+1)f_0, f_y] \tag{21}$$

The spectrum distribution of STF with the existence of linear carrier is shown in Fig. 1(c), where there are lots of lobes distributed at the different locations decided by their parameters k and n. Since f_0 is very large (it equates 1/4 of the whole length along the f_x direction in the frequency domain), the lobes which have the potential to overlap with $S+1$ are all in the $f_x=f_0$ plane as shown in Fig. 1(d). In addition, the amplitude of $E_{\pm k}$ is a module of the vector sum, so the inequality

$$\left|\frac{E_{\pm k}}{S_{\pm 1}}\right| \le \frac{kb_{\pm k}}{Mb_{\pm 1}}\sum_{m=0}^{M-1}|r_m| \tag{22}$$

is satisfied. Usually the amplitude of $b_{\pm k}$ is evidently less than $b_{\pm 1}$ for $k \ge 2$, and r_m is a small value compared with 2π, so the

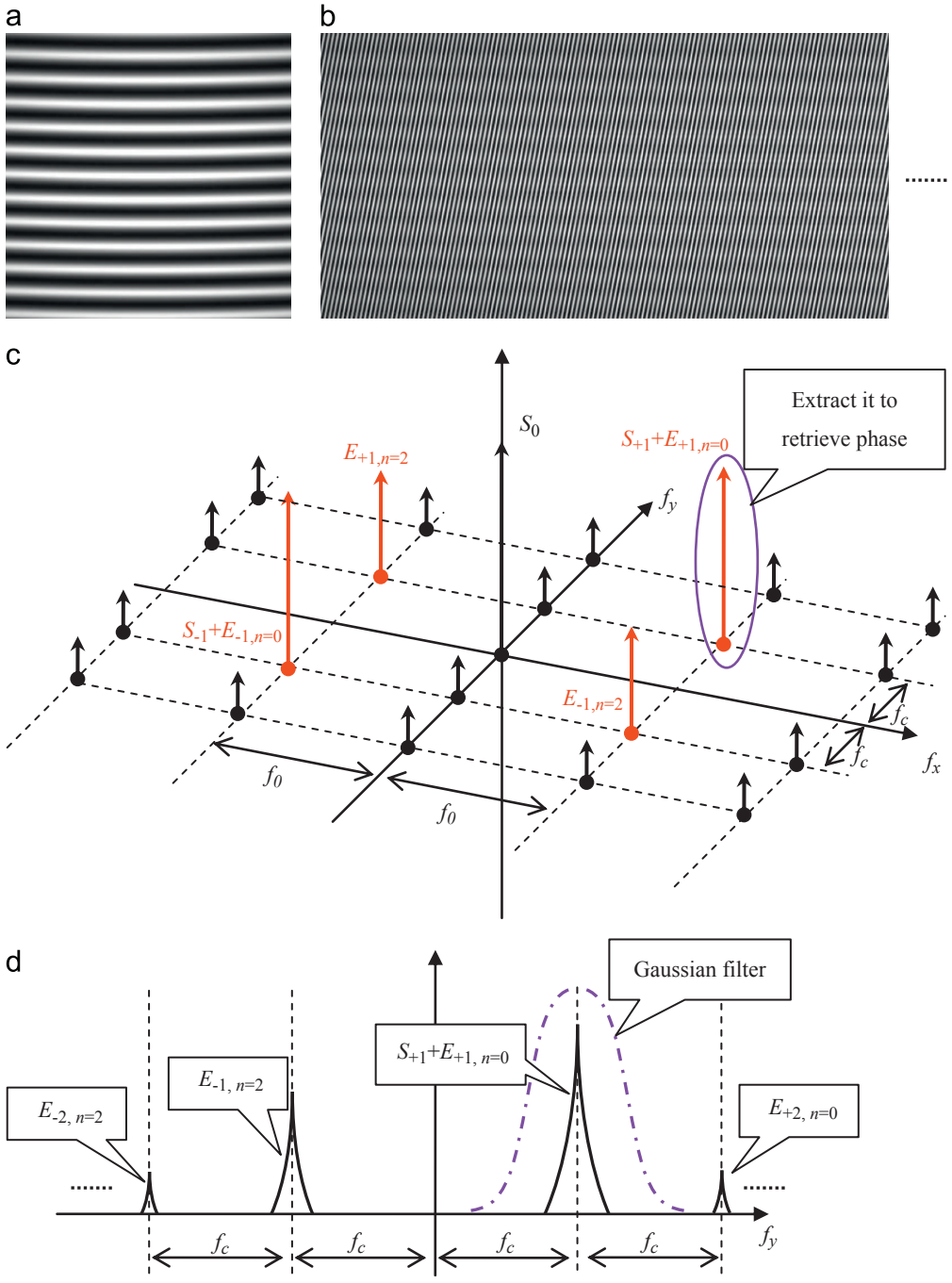

Fig. 1. The principle of the CSI algorithm. (a) The original interferogram. (b) The STF (only the left half of the image is shown). (c) The schematic diagram of the STF spectrum. (d) The $f_x=f_0$ plane of (c) viewed from the $+f_x$ direction.

effect of the error lobes $E_{\pm k}$ to the phase retrieving can be omitted when $k \geq 2$. In other words, although there are many error lobes caused by high order harmonics in the $f_x=f_0$ plane, most of them can be disregarded for their tiny magnitude except for $E_{\pm 1}$; and these two error lobes can be obtained from Eqs. (20) and (21) by substituting $k=1$:

$$E_{+1,n=0} = \frac{-1}{M}\sum_{m=0}^{M-1} r_m S_{+1}(f_x, f_y) \tag{23}$$

and

$$E_{-1,n=+2} = \frac{+1}{M}\sum_{m=0}^{M-1} r_m \exp(-i4\pi m f_0) S_{-1}(f_x - 2f_0, f_y) \tag{24}$$

From Eq. (23) it can be seen that the lobes $E+1$, $n=0$ and $S+1$ are at the same location, and the former equates to the later multiplied by a real number, that is

$$S'_{+1} = S_{+1} + E_{+1,n=0} = R_1 \times S_{+1}(f_x, f_y) \tag{25}$$

where the real number factor $R_1 = 1 - \sum_{m=0}^{M-1} r_m / M$. Therefore, this superposition only changes the amplitude of $S+1$ which will not affect the phase retrieving. On the other hand, $E-1$, $n=+2$ equates to $S-1$ multiplied by a real number; hence, its overlapping with $S+1$ will result in the phase retrieving error. However, the distance between $E-1$, $n=+2$ and $S+1$ is $2f_c$, so these two lobes can be separated from each other if the carrier f_c is suitable. Then the phase lobe $S'+1$ can be extracted independently by a filter window $G(f_x, f_y)$ and the phase can be retrieved by

$$\varphi' = \tan^{-1}\frac{\mathrm{Im}\{FT^{-1}[S(f_x,f_y) \times G(f_x,f_y)]\}}{\mathrm{Re}\mathrm{Im}\{FT^{-1}[S(f_x,f_y) \times G(f_x,f_y)]\}} \tag{26}$$

where $FT^{-1}[\cdot]$ represents the inverse Fourier Transform, while $\mathrm{Re}[\cdot]$ and $\mathrm{Im}[\cdot]$ are the operators to get the real part and imaginary part. The filter used to extract the phase lobe in the CSI can be the Gaussian lowpass filter, which was demonstrated useful in the SI method by Servin et al. [20]:

$$G(f_x,f_y) = \exp\left\{-\left[\frac{(f_x-f_0)^2}{(M\sigma)^2} + \frac{(f_y-f_c)^2}{\sigma^2}\right]\right\} \tag{27}$$

where σ is the parameter to control the bandwidth of the filter window. Experientially σ can be set as $N/10$ and N is the width or height of the original interferogram. Using this convenient estimated value of σ, the retrieved phase is very close to the one using the optimal σ in most situations.

Finally the extensive phase φ' can be recovered to the original size by Eq. (7). So the ability of CSI to suppress both the phase shift errors and the harmonics is demonstrated.

2. The carrier condition

In the previous section the principle of the algorithm is presented, but the necessary linear carrier value is still unknown, which will be analyzed in this section.

It is well known that to demodulate a single linear carrier interferogram using the *FT* method [22], the following carrier condition should be satisfied to separate $S_{\pm 1}$:

$$f_c > \frac{1}{2\pi}\left|\frac{\partial\phi}{\partial y}\right|_{\max} \tag{28}$$

where the carrier is along the y direction. It is an evident conclusion since the two lobes have the same amplitude. However, the situation is different in CSI where the amplitudes of the phase lobe $S'+1$ and the error lobe $E-1$ are different. if the phase shift errors r_m is in the range of $\pm 15^\circ$ and r_0 is considered as zero (since only the relative phase is measured), the amplitude ratio of these two lobes is greater than 5.7 with 99.73% probability through a simple numeric simulation.

Naturally the necessary carrier to separate these two lobes will be less than the situation of Eq. (28), but its value is decided by the phase shape. Since only an approximate estimation of the carrier is needed, we simplify this problem by assuming that the lobes obey the normal distribution and using only a 1D model. As shown in Fig. 2, the overlap area (energy) of two Gauss function with different amplitudes is used to estimate the necessary carrier. The carrier values f_c and f_c' are the distances between two lobes with the equal overlap area but unequal amplitude ratios. The value of f_c'/f_c is 0.86 if the overlap area 1% and 0.92 if the overlap area is 0.1%, so $f_c'=0.9f_c$ can be accepted as an approximated estimation.

However, it is notable that Eq. (28) is only the carrier condition for the ideal interferogram, that is, the background intensity is uniform and there is no harmonics. With these noise, the necessary carrier of *FT* method will be quite different but they do not affect CSI method as we have demonstrated in the previous section. This contrast is shown in Table 1, where it can be seen that the necessary carrier increases evidently in the *FT* method for the non-ideal interferograms but does not change in the CSI method. For example, if there are 2nd-order harmonics in the interferogram, the carrier greater than three times of f_c is

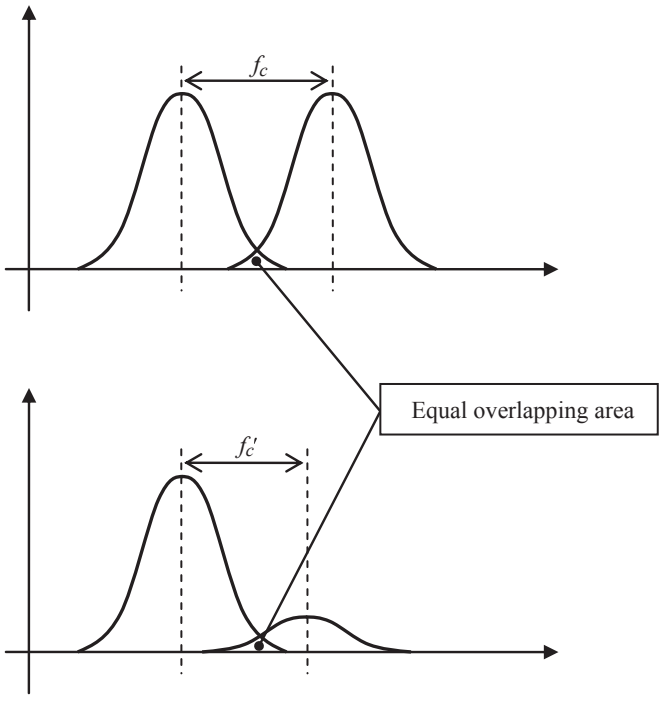

Fig. 2. The difference between the separating of two spectrum lobes with equal and unequal amplitudes.

Table 1
The necessary carrier in the *FT* method and CSI method under the different conditions.

Interferogram conditions	Necessary carrier	
	FT method	CSI method
Ideal interferogram	f_c	$0.9f_c$
With non-uniform background	f_c+f_a[a]	
With qth order harmonics	$(2q-1)f_c$	

[a] f_a is the cutoff frequency of the background component.

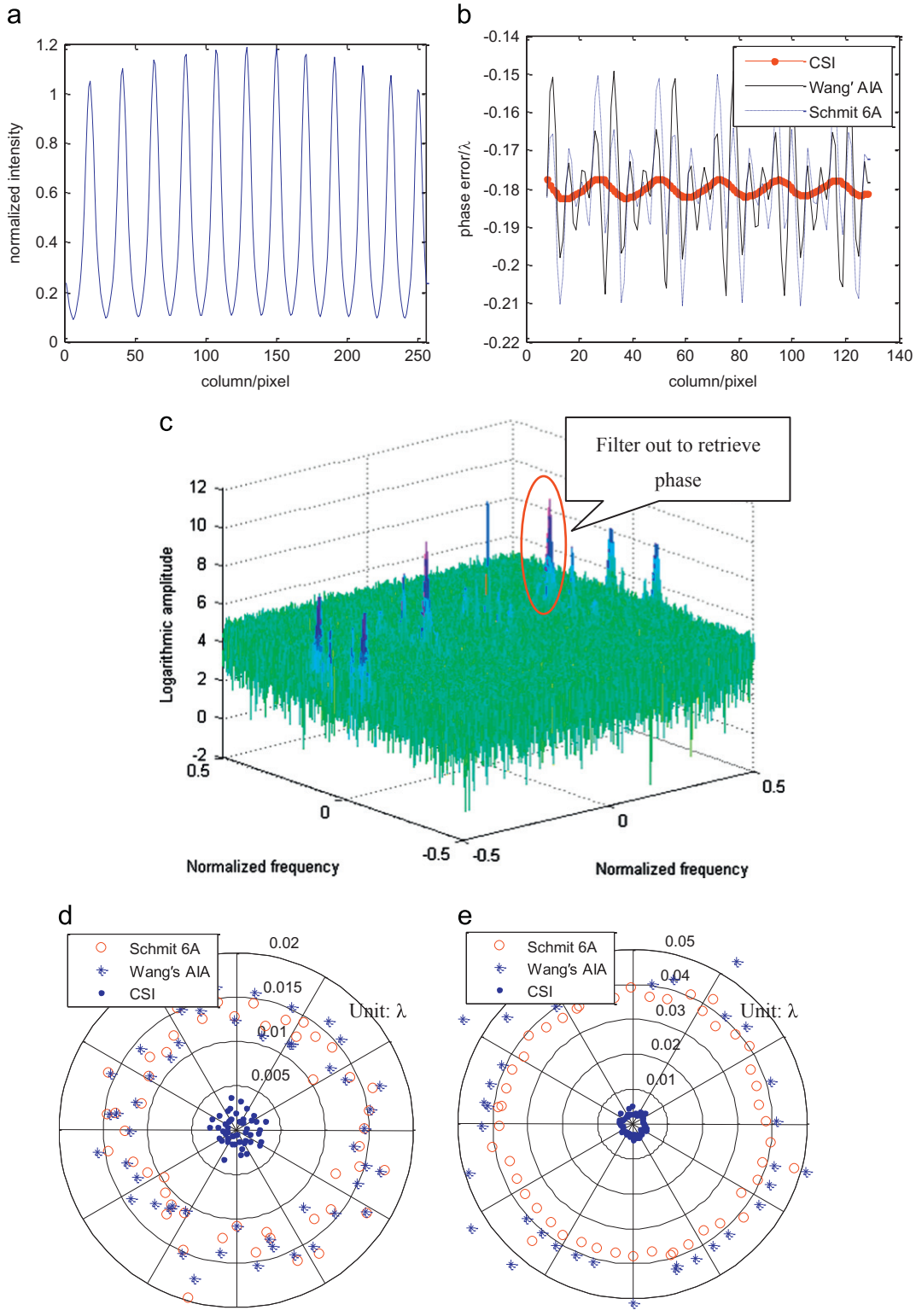

Fig. 3. Simulations. (a) One column of the simulated interferogram (with harmonics). (b) The phase retrieved errors of three algorithms. (c) The frequency spectrum of the STF (using logarithmic amplitude). The distribution of the error RMS values of the three algorithms for the interferograms without (d) and with (e) noise.

necessary to retrieve the phase by *FT* method (considering the non-uniform background). This rigorous demanding usually results in a very large tilt of the reference mirror in the interferometer, which makes the retrace error increase significantly. But using CSI method the necessary carrier is always $0.9f_c$, which is an advantage compared with the *FT* method.

In this section the carrier condition of the CSI method is discussed semi-quantitatively, and the fact is validated that the necessary carrier of CSI is smaller than that of *FT* method (slightly for the ideal interferogram but significantly for the interferogram with non-uniform background and harmonics). Theoretically, we can increase the linear carrier for the object with more high

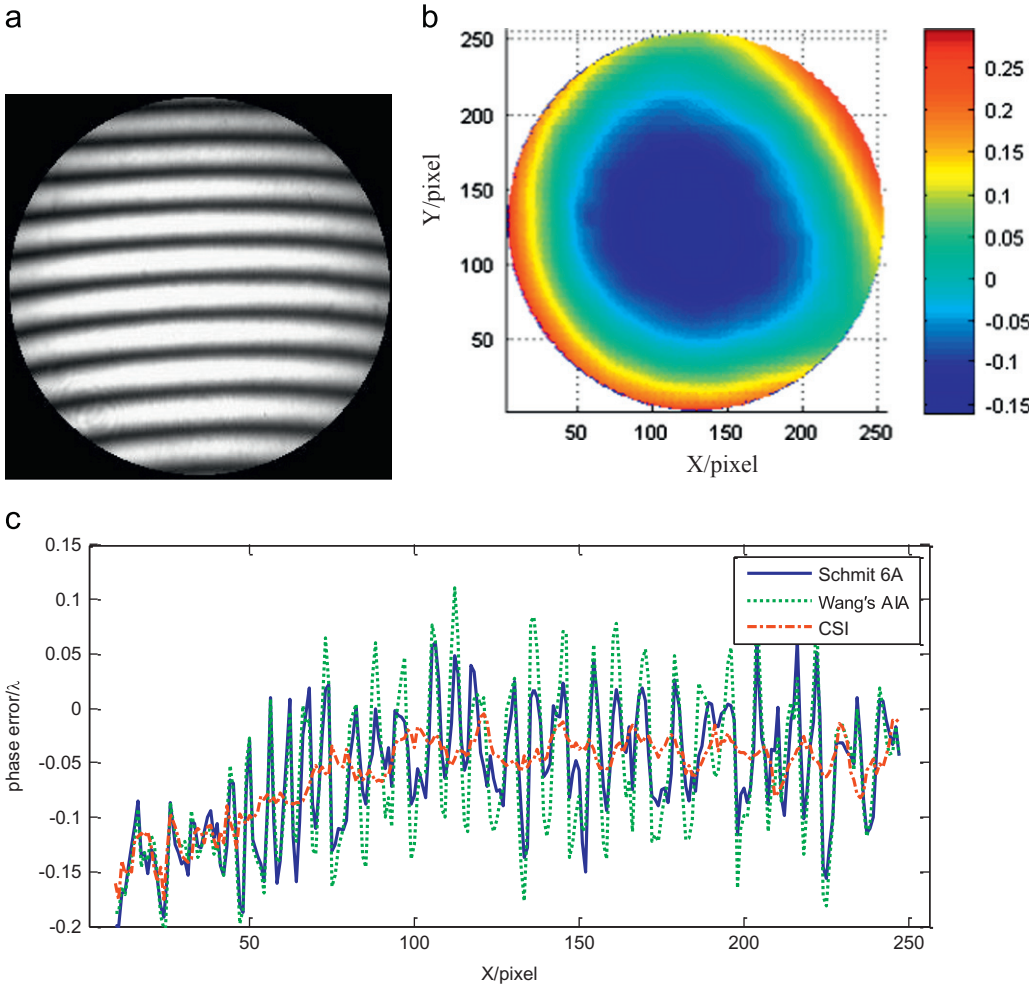

Fig. 4. Experiments using the Zygo phase shifting interferometer. (a) Interferogram captured in the phase shifting interferometer. (b) Retrieved phase by CSI (unit: λ). (c) Phase errors of the central column by three algorithms.

frequency components to satisfy the carrier condition so the maximum phase gradient is only limited by the Nyquist frequency, which is similar as the *FT* method based on the linear carrier. However, there will be a significant retrace error if the tilt is too large. In some references, such as the Zygo "FlashPhase" application manual, there are often 40 fringes approximately in the interferogram if the linear carrier is necessary. That means the maximum phase gradient should be smaller than $2.28\times10-4$ (or $0.36\ \lambda$/mm when $\lambda=0.6328\ \mu$m), so the CSI method is still not suitable for demodulating the phase containing numerous high frequency components such as the step surface.

3. Simulations and experiments

The simulations are executed for verifying the algorithm. The ideal phase step of the simulated interferograms is $\pi/2$, and the non-uniform intensity distribution in each interferogram is assumed as the Gauss Function so that the contrast of the aperture edge is about half of the central one as shown in Fig. 3(a). There are both the phase shift errors (distributed in the range of $\pm15^\circ$) and high order harmonics (with the coefficients $b_2=0.3b_1$ and $b_3=0.3b_2$) in the simulated interferograms, where the assumptions of the errors amplitudes are based on the two factors: (1) Generally speaking, most errors in the actual measurements are at this level; (2) The error suppression ability of the CSI algorithm trends to be decreased when the errors exceed this range. The object phase is set to contain the primary aberrations with the random coefficients, but their peak to valley value is set to be smaller than 1λ. The primary aberrations are defined by the Kingslake polynomial [2]:

$$W(x,y)=A(x^2+y^2)^2+By(x^2+y^2)+C(x^2-y^2)+D(x^2+y^2) \tag{29}$$

where *A*–*D* are the coefficients of spherical aberration, coma, astigmatism and defocusing. The interferograms are processed by the CSI algorithm, the Schmit 6A algorithm (well known for its harmonics suppression ability) [3] and the Wang's advanced iterative algorithm (AIA, insensitive to the phase shift errors) [6] for contrast. Temporally there is no random noise in the interferogram since the Schmit 6A algorithm and Wang's AIA are not insensitive to it. As a intermediate result, the frequency spectrum of the STF is shown in Fig. 3(c), where the logarithmic amplitude of the spectrum is used to display the small lobes clearly. In this figure, we can see that the phase lobe can be extracted independently to retrieve the phase, which is the same as the conclusion of Section 2.

The phase error of one column is shown in Fig. 3(b), where the amplitudes of phase errors obtained by Schmit 6A algorithm and Wang's AIA are almost the same while the CSI algorithm has a much less one, because the former two algorithm can suppress only one kind of error while CSI suppresses two kinds of errors simultaneously. Totally 50 groups of simulation results are obtained, where the RMS values of phase retrieving error of the three algorithm are shown in Fig. 3(c). It can be seen that the

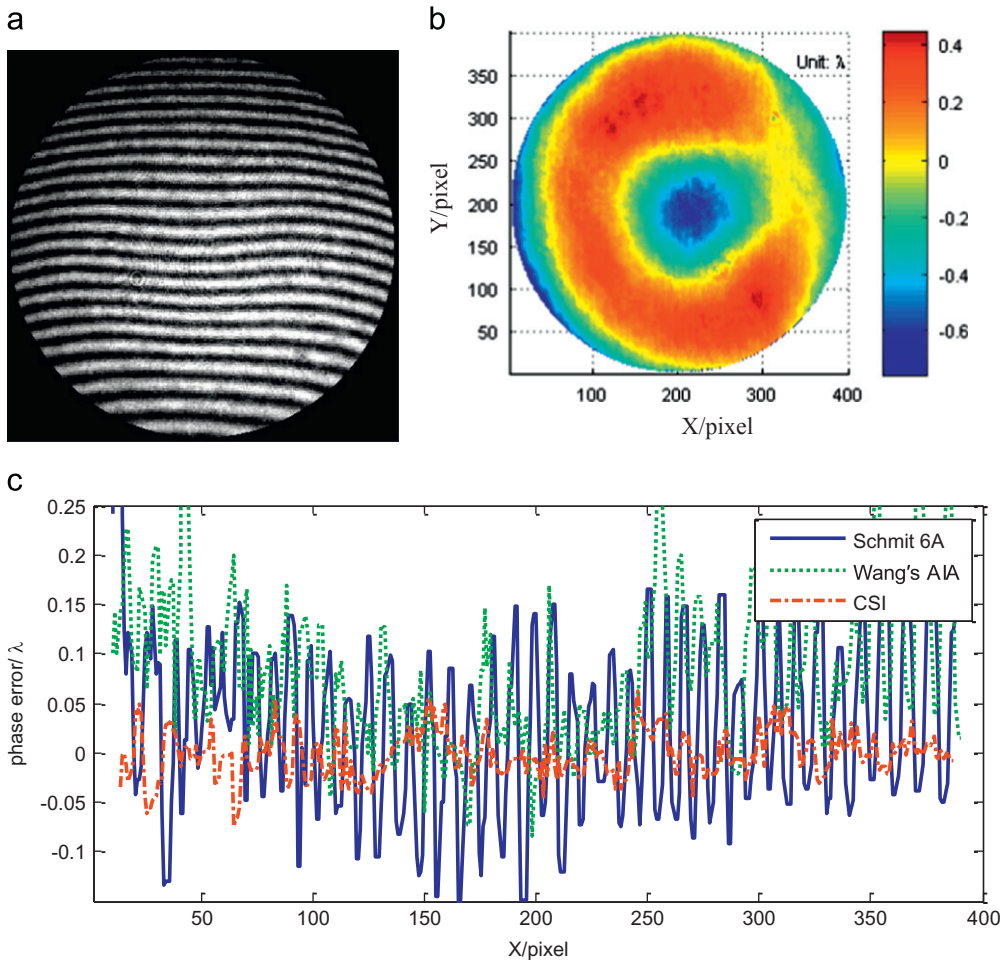

Fig. 5. Experiments using the 4D dynamic interferometer. (a) Interferogram captured in the phase shifting interferometer. (b) Retrieved phase by CSI (unit: λ). (c) Phase errors of the central column by three algorithms.

phase errors of CSI are always less than 0.004λ and the mean error is 0.0017λ, while the mean errors of Schmit 6A algorithm and Wang's AIA are 0.0137λ, and 0.0132λ, respectively.

With the existence of random noise, the error suppression ability of CSI is more powerful compared with the other two algorithms for its inherited low-pass filtering characteristic. As shown in Fig. 3(e), the results of CSI keep high accuracy (mean value of phase error RMS is 0.0026λ) for the interferograms with the SNR of 10:1, while the phase retrieving errors of other two algorithms are much worse than the error-free conditions with the mean error of 0.039λ. Although the results of Schmit 6A algorithm and Wang's AIA can also be improved by an extra low-pass filtering to overcome the random noise, the calculation of CSI is more direct.

In the experiments, first a flat mirror with the aperture of 100 mm is tested by a Zygo GPI-XP interferometer to capture the phase shifting interferograms, where the intensity saturation is introduced to generate harmonics. Besides, the air compressor used for the vibration–isolation supports of the optical table is turned off so that the vibration can be introduced to generate the phase shift error. The Schmit 6A algorithm, Wang's AIA and our CSI algorithm are used to process these interferograms whose results are compared with the standard phase obtained under the normal measurement conditions. One of the captured interferograms is shown in Fig. 4(a), and the retrieved phase by CSI is shown in Fig. 4(b). To compare the performances of the three algorithms clearly, the central columns of their demodulated errors are shown in Fig. 4(c), where it can be seen that the error amplitude of CSI is significantly less than other two algorithms and the error RMS values of the three algorithms are 0.0036λ, 0.0103λ and 0.0109λ, respectively. Here the data within the 98% aperture are used to calculate the RMS value considering the well known "edge error" of all phase retrieving method based on the *FT* (containing the CSI). The relative errors suppression ability of the CSI compared with other two algorithms seems to be weaker than that in the simulations. It may be caused by the errors that cannot be suppressed by all of the three algorithms, such as the space non-uniform phase shift errors. For example, if this kind of errors results in the phase error RMS value of 0.0025λ, the two errors suppressed by the three algorithms are 0.0011λ, 0.0078λ and 0.0084λ, respectively; and in this case the error suppression ability of CSI compared with other two algorithms is very similar to that of simulations.

Second, a concave mirror with the aperture of 130 mm and the radius of 630 mm is tested using the 4D phaseCam2000 dynamic interferometer in the natural vibration environment, which is able to capture the phase shifting interferograms simultaneously. The interferograms are captured continuously, so the phase shifting interferograms with $\pi/2$ phase shift at different time (i.e., temporal phase shifting interferograms) also can be obtained. These interferograms are set to be over gained so that they contain both the phase shift errors and the harmonics where one of them is shown in Fig. 5(a). The vibration-immune phase are retrieved from the simultaneous phase shifting interferograms as the standard one, and the temporal phase shifting interferograms with over contrast are demodulated by the three

algorithms to compare their error suppression ability. The demodulated phase by CSI is presented in Fig. 5(b) where it can be seen that the phase is more varying than the previous experiment, and the error RMS values of the three algorithms are 0.0173λ, 0.0161λ and 0.0042λ, respectively. The central columns of the demodulation errors of the three algorithms are also shown in Fig. 5(c), which is similar as the former experiment. However, it is notable that the linear carrier in the interferogram is greater this time, since the phase is more varying. If the carrier is the same as the previous experiment (about 12 fringes in the interferogram), the demodulated error (RMS value) will be 0.116λ since the error lobe and the phase lobe overlap in the frequency domain.

4. Conclusion

In this paper the carrier squeezing interferometry (CSI) algorithm is proposed to simultaneously suppress the phase errors in the PSI arising from the inaccurate phase shifts and the harmonics. It is suitable for various phase shift errors (such as the vibrations, the phase shifter distortions and so on) as long as they are spatial uniform since the actual phase shifts are considered as the random values in the algorithm. Besides, any order of harmonics can be rejected if its coefficient b_k is not too large (it cannot be close to b_1 or even greater), which can be satisfied in most cases. An advantage of this method is that only four phase shifting interferograms are used. On the other hand, this method is not suitable for the phase with much component of high frequency (such as the step) because of its inherited low passing filtering.

Acknowledgements

The authors are grateful for the supports of National Natural Science Foundation of China (61108041 and 11003032).

References

[1] J.H. Bruning, D.R. Herriott, J.E. Gallagher, D.P. Rosenfeld, A.D. White, D.J. Brangaccio, Applied Optics 13 (1974) 2693.
[2] D. Malacara, Optical Shop Testing, John Wiley & Sons, New York, 2007.
[3] J. Schmit, K. Creath, Applied Optics 34 (1995) 3610.
[4] P.d. Groot, Applied Optics 34 (1995) 4723.
[5] A. Tellez-Quinones, D. Malacara-Doblado, J. Garcia-Marquez, Journal of the Optical Society of America a-Optics Image Science and Vision 29 (2012) 431.
[6] Z.Y. Wang, B.T. Han, Optics Letters 29 (2004) 1671.
[7] P. Gao, B.L. Yao, N. Lindlein, K. Mantel, I. Harder, E. Geist, Optics Letters 34 (2009) 3553.
[8] K. Okada, Optics Communications 84 (1991) 118.
[9] X.F. Xu, L.Z. Cai, Y.R. Wang, X.L. Yang, X.F. Meng, G.Y. Dong, X.X. Shen, H. Zhang, Applied Physics Letters 90 (2007) 3.
[10] Q. Kemao, H. Wang, W. Gao, L. Feng, S.H. Soon, Optics and Lasers in Engineering 48 (2010) 684.
[11] J. Schwider, R. Burow, K.E. Elssner, J. Grzanna, R. Spolaczyk, K. Merkel, Applied Optics 22 (1983) 3421.
[12] J.M. Huntley, Journal of the Optical Society of America A: Optics, Image Science, and Vision 15 (1998) 2233.
[13] L.L. Deck, Applied Optics 48 (2009) 3948.
[14] H.W. Guo, H.T. He, M. Chen, Applied Optics 43 (2004) 2906.
[15] T. Hoang, B. Pan, D. Nguyen, Z. Wang, Optics Letters 35 (2010) 1992.
[16] S. Ma, C. Quan, R. Zhu, L. Chen, B. Li, C.J. Tay, Optics Communications 285 (2012) 533.
[17] J.C. Xu, Q. Xu, L.Q. Chai, Journal of Optics A: Pure and Applied Optics 10 (2008) 5.
[18] T. Hoang, Z. Wang, M. Vo, J. Ma, L. Luu, B. Pan, Applied Physics Letters 99 (2011).
[19] B. Li, L. Chen, W. Tuya, S. Ma, R. Zhu, Optics Letters 36 (2011) 996.
[20] M. Servin, M. Cywiak, D. Malacara-Hernandez, J.C. Estrada, J.A. Quiroga, Optics Express 16 (2008) 9276.
[21] J.M. Padilla, M. Servin, J.C. Estrada, Optics Express 19 (2011) 19508.
[22] M. Takeda, H. Ina, S. Kobayashi, Journal of the Optical Society of America 72 (1982) 156.